ELSEVIER

Available online at www.sciencedirect.com

ScienceDirect

Nuclear and Particle Physics Proceedings 273–275 (2016) 117–124

www.elsevier.com/locate/nppp

$H \to \gamma\gamma$ measurements at the ATLAS experiment

Kerstin Tackmann

Deutsches Elektronen-Synchrotron (DESY), D-22607 Hamburg, Germany

---

Abstract

Measurements of the Higgs boson properties at the Large Hadron Collider experiments require a thorough understanding and control of the detector performance. These proceedings describe the reconstruction, identification and calibration of photons at the ATLAS experiment, which are of particular importance for the measurements in the diphoton decay channel. The impact on the property measurements is shown, along with the results of the $H \to \gamma\gamma$ measurements.

Keywords: Large Hadron Collider, ATLAS experiment, Higgs boson, diphoton

---

1. Introduction

In July 2012, the ATLAS and CMS collaborations reported the discovery of a new particle in the searches for the Standard Model (SM) Higgs boson [1, 2]. Since then, further measurements and tests of the properties of the new particle have been carried out, taking advantage of an improved understanding of the detectors and the larger datasets recorded until the end of 2012.

2. The ATLAS detector and dataset

The ATLAS experiment is a multipurpose particle physics detector at the Large Hadron Collider (LHC), with a forward-backward symmetric barrel-endcap geometry[1]. It is described in detail in Ref. [3]. The measurements described here rely strongly on the inner tracking detector and the electromagnetic calorimeter.

The inner detector consists of a silicon pixel detector and a silicon microstrip detector, which cover the pseudorapidity range of $|\eta| < 2.5$, as well as a transition radiation tracker (TRT) covering the pseudorapidity range of $|\eta| < 2$. The inner detector is immersed in a 2 T solenoidal magnetic field. It allows an accurate reconstruction of charged-particle tracks originating from the proton-proton interaction region, as well as from secondary vertices. The TRT offers electron identification through transition radiation in scintillating foils and fibers.

The electromagnetic calorimeter is a lead/liquid-argon sampling calorimeter with an accordion geometry. In the region $|\eta| < 2.5$, it is segmented into three longitudinal layers. In the regions $|\eta| < 1.4$ and $1.5 < |\eta| < 2.4$, the innermost layer is segmented into narrow strips in the η direction, allowing a measurement of the internal structure of the electromagnetic shower. The second layer collects most of the energy deposited by electrons and photons in the calorimeter. In the region $|\eta| < 1.8$, a thin presampler layer in front of the accordion calorimeter is used to correct for energy loss upstream of the calorimeter.

The data samples amount to about $4.5\,\text{fb}^{-1}$ and $20.3\,\text{fb}^{-1}$ recorded at $\sqrt{s} = 7$ TeV and $\sqrt{s} = 8$ TeV, respectively, after the application of data-quality requirements. The data was taken with an average number of interactions per bunch crossings of 9 ($\sqrt{s} = 7$ TeV) and 21 ($\sqrt{s} = 8$ TeV).

---

[1] ATLAS uses a right-handed coordinate system with its origin at the nominal interaction point (IP) in the center of the detector and the z-axis along the beam pipe. The x-axis points from the IP to the center of the LHC ring, and the y-axis points upward. Cylindrical coordinates (r, ϕ) are used in the transverse plane, ϕ being the azimuthal angle around the beam pipe. The pseudorapidity is defined in terms of the polar angle θ as $\eta = -\ln[\tan(\theta/2)]$.

http://dx.doi.org/10.1016/j.nuclphysbps.2015.09.014

3. Overview of the $H \to \gamma\gamma$ measurements

Detailed descriptions of the $H \to \gamma\gamma$ measurements from the ATLAS experiment can be found in Refs. [4, 5, 6]. They describe the measurement of the Higgs boson mass in the diphoton and $H \to 4\ell$ decay channels [4], the study of the Higgs boson production modes [5][2], and the measurements of fiducial and differential cross sections in $H \to \gamma\gamma$ decays [6]. The measurements are based on data samples collected using a diphoton trigger. Events are required to contain at least two reconstructed photon candidates in the fiducial region of the calorimeter, $|\eta| < 1.37$ or $1.56 < |\eta| < 2.37$. The barrel-endcap transition regions, $1.37 < |\eta| < 1.56$, are excluded. The leading photon candidate is required to have a transverse energy $E_T > 0.35 m_{\gamma\gamma}$, and the subleading candidate is required to have $E_T > 0.25 m_{\gamma\gamma}$. Tight identification criteria (discussed in more detail in Sec. 4) are applied to both photon candidates. Furthermore, the photon candidates are required to be isolated in the calorimeter and inner tracking detector. The efficiency to select $H \to \gamma\gamma$ events is estimated from simulation to range from 32 to 42% depending on the production mode.

Figure 1 shows the diphoton invariant mass spectrum of the selected events in the $\sqrt{s} = 7$ and 8 TeV data sets. The signal is clearly visible as a narrow peak on top of a smoothly falling background. The background subtraction is performed by parametrizing the background with an analytic function. The parametrization has been chosen to have only a small systematic bias on the measured signal event yield (or the resonance invariant mass, in the case of the mass measurement) compared to the statistical uncertainty.

To obtain a high signal yield and a good signal-to-background ratio, the measurements in the diphoton final state require a large reconstruction and identification efficiency for photons, and a large rejection of the dominant hadronic backgrounds from dijet and γ-jet production (discussed in Sec. 4). Furthermore, to obtain a narrow signal peak, a good resolution of the diphoton invariant mass, $m_{\gamma\gamma} = \sqrt{2E_1E_2(1 - \cos\alpha)}$, with α the opening angle between the two photons, is needed. This in turn requires a good resolution of the photon energy (discussed in Sec. 5) and direction (see below). Finally, the measurement of the Higgs boson mass requires a precise calibration of the photon energy (see Sec. 5).

For the measurement of the photon direction and the selection of jets originating from the same proton-proton interaction as the diphoton pair, the primary vertex of the hard interaction is identified. This is achieved by combining a measurement of the photon direction, making use of the longitudinal segmentation of the calorimeter and the position of the conversion vertex if the tracks have hits in the silicon detectors (for converted photons), the $\sum p_T^2$ and the $\sum p_T$ of the tracks associated with each primary vertex and the difference in azimuthal angle between the direction of the diphoton system and the tracks associated with the given primary vertex. The contribution of the photon direction measurement to the resolution of the invariant mass of the diphoton pair is negligible.

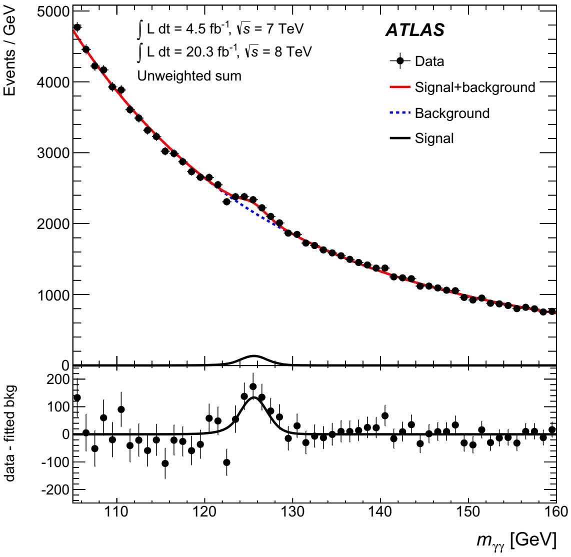

Figure 1: Diphoton invariant mass spectrum, combining the data taken at $\sqrt{s} = 7$ and 8 TeV shown as data points, together with the parametrization of the background (blue dashed) and the sum of the signal and background parametrizations (red) [5]. The lower plot shows the difference between the data and the parametrized background, as well as the parametrization of the signal (black).

4. Photon reconstruction and identification

A high photon reconstruction and identification efficiency is essential to achieve a high efficiency for reconstructing $H \to \gamma\gamma$ decays.

Due to the rather large amount of detector material in front of the calorimeter, about 40% of photons coming from a $H \to \gamma\gamma$ decay convert to an electron-positron pair before reaching the calorimeter. A good separation of unconverted and converted photons in the reconstruction is needed to ensure the best possible performance

---

[2] These proceedings present the results published in Ref. [5], which became available shortly after ICHEP 2014.

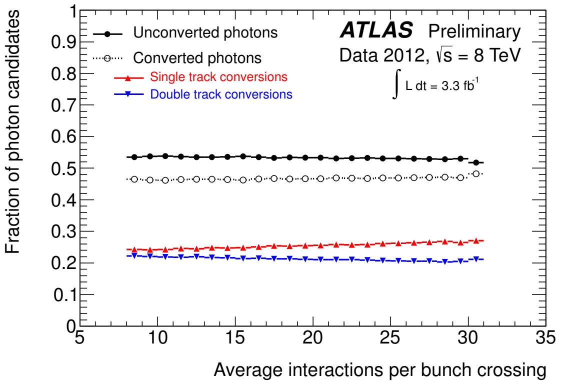

Figure 2: Stability of the photon conversion reconstruction for a wide range of average interactions per bunch crossing for the $\sqrt{s} = 8\,\text{TeV}$ data [8]. The fraction of photon candidates reconstructed as unconverted photons (black, full) and converted photons (black, open) is shown. For converted photon candidates, the contribution from candidates reconstructed as single-track converted photons (red) and as double-track converted photons (blue) is separated.

of the identification and of the energy calibration of both photon types.

The photon reconstruction is seeded from clusters of energy deposits in the electromagnetic calorimeter. Converted photons are reconstructed by matching conversion vertices formed from two (double-track conversion) or one track (single-track conversion) to the electromagnetic cluster. For the $\sqrt{s} = 8\,\text{TeV}$ data, double-track vertices are formed from tracks that have been loosely matched to electromagnetic clusters, and, if they have a sufficient number of hits in the silicon detectors, refitted with a Gaussian Sum Filter [7] to improve the track-parameter resolution. Single-track vertices are formed from tracks with a high probability to be an electron, based on transition radiation in the TRT, and missing a hit in the innermost pixel layer. Track and vertex reconstruction, as well as vertex-cluster matching criteria have been tightened for the $\sqrt{s} = 8\,\text{TeV}$ data for improved pileup robustness. Converted photon candidates reconstructed from tracks passing through dead modules of the innermost pixel layer are rejected, strongly decreasing the misidentification of electrons as converted photons. Unconverted photons are reconstructed from clusters without a matching track or conversion vertex. On average, the reconstruction efficiency for photons with $E_T > 25\,\text{GeV}$ is $\sim 96\%$.

Figure 2 shows the fraction of photon candidates reconstructed as unconverted photon, as single- and as double-track conversion as a function of the number of average interactions per bunch crossing for the $\sqrt{s} = 8\,\text{TeV}$ data. The reconstruction is stable over a wide range of pileup.

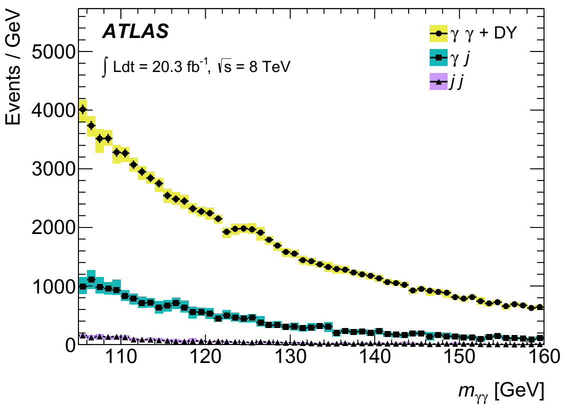

Figure 3: Composition of the selected diphoton sample in the 8 TeV data [5], showing the contribution of $\gamma\gamma$ and Drell-Yan events (yellow), γ–jet (blue) and jet–jet events (violet).

Due to the large jet production cross section, a large fraction of the reconstructed photon candidates are hadronic jets misreconstructed as photons. To achieve a good diphoton purity and reduce the γ–jet and jet–jet backgrounds well below the irreducible $\gamma\gamma$ background in the $H \to \gamma\gamma$ measurements, jet rejection factors of a few 10^3 are needed. The identification of photons is based on variables that describe the shape of the electromagnetic shower in the calorimeter. An initial loose selection, used also at the trigger level, is based on rectangular cuts on variables parametrizing the shower shape in the second layer of the electromagnetic calorimeter, as well as the energy deposition in the hadronic calorimeter. A tight identification adds information from the finely segmented strip layer of the calorimeter, which provides good rejection of hadronic jets where a neutral meson carries most of the jet energy. Two variants of the tight identification are used. For the $\sqrt{s} = 7\,\text{TeV}$ data, a neural-network based selection is used. For the $\sqrt{s} = 8\,\text{TeV}$ data, a cut-based selection is used, which was tuned for robustness against pileup effects. In the $\sqrt{s} = 8\,\text{TeV}$ data, the identification efficiency for unconverted and converted photons ranges between 83–95% and 87–99%, respectively, depending on E_T and $|\eta|$.

Figure 3 shows the contributions of $\gamma\gamma$, γ–jet and jet–jet events to the selected diphoton sample, as obtained from a two-dimensional sideband method [9]. In the 8 TeV data, the fraction of $\gamma\gamma$ events is about $77 \pm 3\%$.

The photon identification efficiency for isolated photons is measured on data using three different methods, with partially overlapping E_T range [10]. In the

ICHEP 2012 [1]	10.8%
December 2012 [12]	5.3%
Moriond 2013 [13]	2.4%
ICHEP 2014 [5]	1%

Table 1: Evolution of the systematic uncertainty on the signal yield in $H \to \gamma\gamma$ signal strength measurements coming from the uncertainties on the photon identification efficiency measurement.

lowest E_T range, from 10 to 80 GeV, a tag-and-probe measurement using radiative Z-boson decays, $Z \to \ell\ell\gamma$ ($\ell = e, \mu$), is carried out. Above $E_T = 15$ GeV, a photon purity of larger than 98% can be achieved. In the intermediate E_T range, a tag-and-probe measurement based on $Z \to ee$ is used, making use of the similarity of electromagnetic showers from electrons and photons ("electron extrapolation"). Differences between electron and photon shower shapes are taken into account by shower shape transformations derived from simulation (see Fig. 4 for an example). The uncertainties on the identification efficiency measurement from this method are dominated by the uncertainties on this transformation. The third method ("matrix method"), covering the E_T range from 20 GeV to 1.5 TeV, makes use of the isolation of photon candidates in the inner detector to determine the sample purity before and after the application of tight identification cuts. The systematic uncertainties on the measured identification efficiency are dominated by uncertainties on the data–simulation differences of the track isolation.

Since the measurements are found to agree well in the overlapping E_T ranges (see Fig. 5), their results are combined and used to derive efficiency correction factors applied on the $H \to \gamma\gamma$ simulation. The absolute uncertainties on the measured identification efficiencies range from 1 – 2% for $E_T < 40$ GeV to 0.5 – 1% above 40 GeV.

Table 1 shows the evolution of the photon identification efficiency systematic uncertainty on the $H \to \gamma\gamma$ signal yield in several steps from the discovery [1] to the measurement presented here. The reduction of the uncertainty by about an order of magnitude was made possible by commissioning and improving all methods described above, and by improving the model used to correlate the uncertainties between the two photons in the event. Thanks to this reduction, the uncertainty on the photon identification efficiency (in the $\sqrt{s} = 8$ TeV analysis) is no longer among the largest experimental uncertainties in the $H \to \gamma\gamma$ signal strength measure-

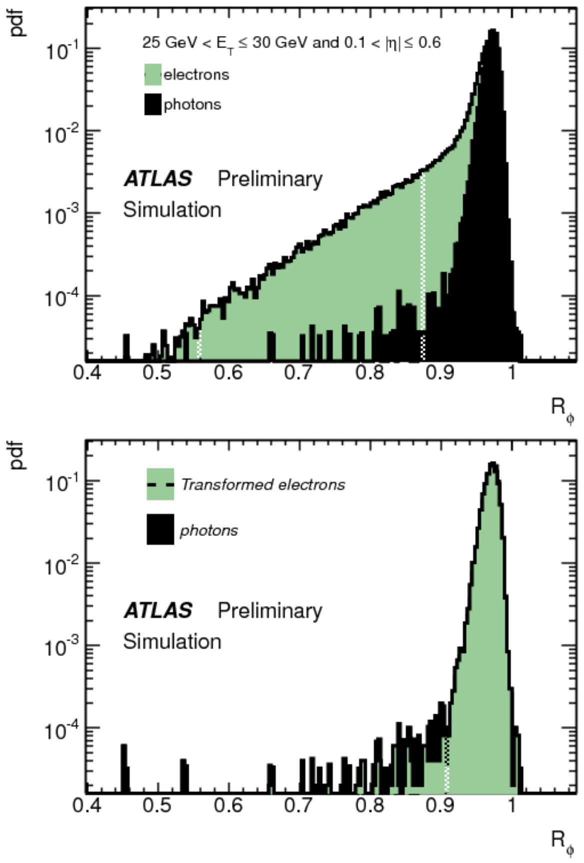

Figure 4: Shower shape variable R_ϕ, which measures the width of the shower in ϕ direction in the second layer of the calorimeter, for electrons (green) and photons (black) before (top) and after (bottom) a transformation has been applied to the electron R_ϕ.

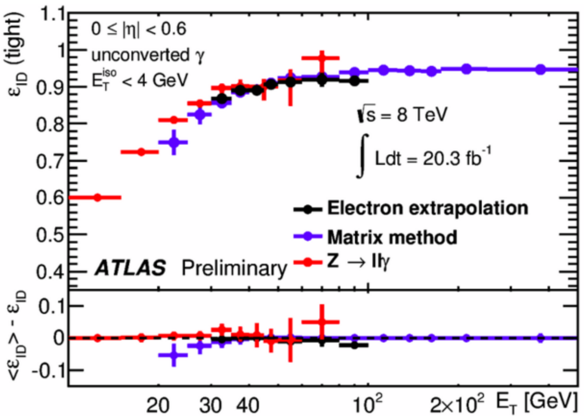

Figure 5: Photon identification efficiency for isolated, unconverted photons in the range $0 < |\eta| < 0.6$ as measured with the different methods, using radiative Z-boson decays, $Z \to \ell\ell\gamma$ (red), extrapolating from electrons in $Z \to ee$ events (black) , and the matrix method (blue), described in the text, for the $\sqrt{s} = 8$ TeV dataset [11].

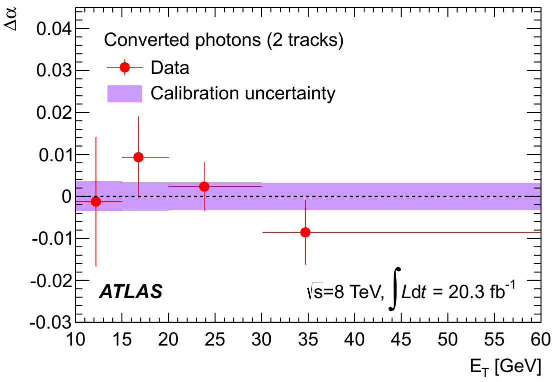

Figure 6: Cross check of the energy calibration derived from $Z \to ee$ events with double-track converted photons from radiative Z-boson decays, $Z \to \ell\ell\gamma$ [14]. $\Delta\alpha$ is the absolute energy scale measured after the nominal scale corrections measured in $Z \to ee$ are applied. The measurement (red) is compared to the uncertainty on the energy calibration from $Z \to ee$ (violet).

ment, where the signal strength is defined as the ratio of the measured number of events to the number of events expected from the SM.

5. Photon energy calibration and resolution

A precise energy calibration as well as a high and well-understood resolution are crucial for Higgs boson measurements. A good energy resolution is needed to obtain a narrow signal peak. The mass measurement requires also a very precise energy calibration, while the measurement of the signal strength needs a well-understood resolution.

The energy calibration procedure for photons is carried out in several steps [14]. After the initial application of corrections to account for response details of the calorimeter not modeled by the simulation, such as corrections for regions not operated at the nominal high voltage, a simulation-based energy calibration is applied separately to unconverted and converted photons, and electrons. The calibration constants are derived with a multivariate algorithm, using the longitudinal shower development, the position of the cluster in the calorimeter, and additional information from the inner tracking detector for converted photons. In the next step, the response of the longitudinal layers of the calorimeter is equalized, following measurements of the relative energy scales of the different layers with muons, electrons and unconverted photons. This equalization ensures the correct extrapolation of the response to a wide range of energies. As a last step, the absolute energy scale is corrected as derived from $Z \to ee$ decays. Together with the absolute energy scale, a resolution correction is derived, which is applied to the simulation.

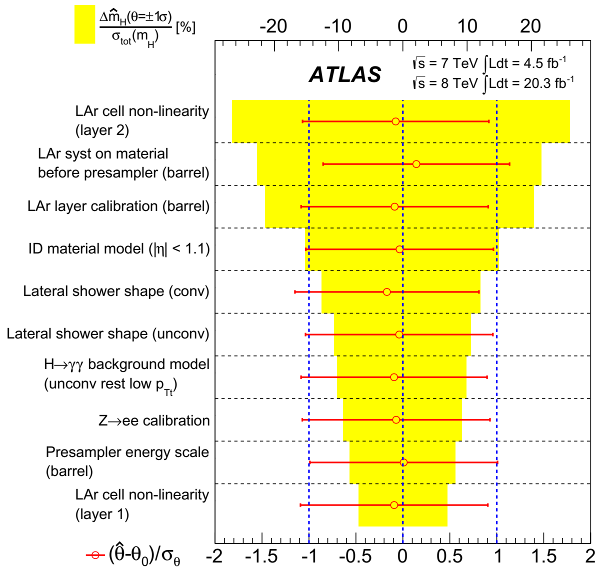

Figure 7: Dominant systematic uncertainties in the Higgs boson mass measurement [4]. The yellow shaded areas show the relative change in the fitted mass from varying the parameter associated to a given uncertainty by its fitted uncertainty. The red points and error bars show the fitted value and uncertainty for the associated parameter.

The new multivariate energy calibration improves the diphoton invariant mass resolution for $H \to \gamma\gamma$ decays by about 10% compared to the previous calibration [15, 13].

The use of a simulation-based energy calibration requires an accurate simulation of the detector material in front of the calorimeter. The simulation has been tested and improved by studying longitudinal shower shapes of electrons and unconverted photons. In most regions of the detector, these studies constrain the material in front of the calorimeter to $4-6\% X_0$.

The absolute energy scale is cross checked using photons from radiate Z-boson decays and found to agree within uncertainties (see Fig. 6).

The systematic uncertainty on the photon energy scale for photons with $E_T = 60$ GeV ranges from 0.18 to 1.35%, depending on the $|\eta|$ region, and is 0.3% on average. The impact of the dominant contributions to the systematic uncertainty in the Higgs boson mass measurement is shown in Fig. 7. The largest sources are an observed cell non-linearity in the second layer of the calorimeter, the systematic uncertainty associated to the knowledge of calorimeter material in front of the presampler layer, and the uncertainties on the relative energy scales of the first and second layer of the calorime-

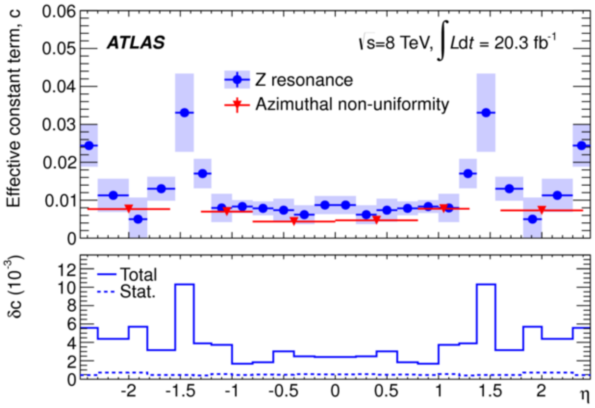

Figure 8: Effective constant term of the calorimeter resolution derived from $Z \to ee$ events (blue) with statistical and systematic uncertainties (light blue and bottom). The values and uncertainties are symmetrized with respect to $\eta = 0$. The contribution from the response uniformity of the calorimeter is included for comparison [14] (red).

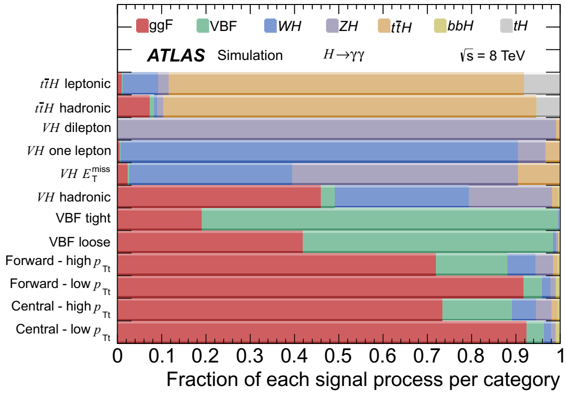

Figure 9: Event categories in the $H \to \gamma\gamma$ coupling measurement as described in the text, and expected contributions of the different production modes in the SM [5].

ter.

The systematic uncertainty on the photon energy resolution is the largest contribution to the experimental systematic uncertainty on the measurement of the Higgs boson signal strength. Uncertainties arise from the measurement of the resolution in $Z \to ee$ events (see Fig. 8), the modeling of the detector material in the simulation, the knowledge of the sampling term in the calorimeter resolution from test beam measurements, and the effect of pileup.

6. Higgs boson mass measurement

The Higgs boson mass is measured from the position of the $H \to \gamma\gamma$ peak in the diphoton invariant mass spectrum. For this measurement, the events are split into 10 categories for each of the $\sqrt{s} = 7\,\text{TeV}$ and $\sqrt{s} = 8\,\text{TeV}$ data samples, according to the $|\eta|$ position of the photons in the calorimeter, whether or not the photons converted in the inner detector, and the p_{Tt} of the diphoton system [16].

The mass is measured to be

$$m_H = (125.98 \pm 0.42(\text{stat}) \pm 0.28(\text{syst}))\,\text{GeV [4]}.$$

The systematic uncertainty, dominated by the systematic uncertainty on the photon energy scale, was reduced by about a factor of 2.5 compared to the previous measurement [13].

7. Separation of Higgs boson production modes

In the SM, the couplings between the Higgs boson and the vector bosons and fermions are determined by the vector boson and fermion masses. These couplings can be measured, or at least constrained, by studying Higgs boson production and decays. In the SM, the Higgs boson is expected to be dominantly produced through gluon fusion (ggF), vector boson fusion (VBF), and associated production with a vector boson (W or Z) or a $t\bar{t}$ pair.

To separate the contributions of the different production processes, the measurement splits the event sample into 12 exclusive event categories for each of the $\sqrt{s} = 7\,\text{TeV}$ and $\sqrt{s} = 8\,\text{TeV}$ data samples.

Two categories are defined to have a high purity in $t\bar{t}H$ events. They are enriched in leptonic and hadronic decays of a $t\bar{t}$ pair. The selection requires the presence of at least one lepton (electron or muon), one or two jets tagged as b-jets, and missing transverse momentum, E_T^{miss}, for the *$t\bar{t}H$ leptonic* category, and a minimum number of jets and b-tagged jets for the *$t\bar{t}H$ hadronic* category.

Four categories target the associated production with a vector boson. The *VH dilepton* category requires the presence of two opposite-sign leptons in the event, consistent with coming from a decay of a Z boson. The *VH one-lepton* category requires the presence of one lepton in the event, and makes a requirement on the significance of the missing transverse momentum in the event, E_T^{miss}, to enrich the category in WH events. The *VH E_T^{miss}* category aims to select WH events with leptonic W decays, where the lepton was not reconstructed or selected, and ZH events with $Z \to \nu\bar{\nu}$. In addition to a requirement on the significance of E_T^{miss} in the event, the p_{Tt} is required to be larger than 20 GeV. Finally, the *VH hadronic* category selects events consistent with a

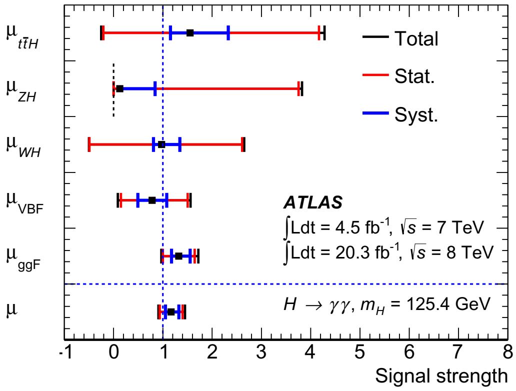

Figure 10: Signal strength measured for the different Higgs boson production modes and the contribution of the statistical (red) and systematic and theoretical (blue) uncertainties to the total uncertainty (black). In the bottom, the inclusive signal strength is shown [5].

hadronic decay of a W or Z boson.

Two categories, *VBF tight* and *VBF loose* are enriched in vector boson fusion production, using a boosted decision tree (BDT). The BDT is based on six variables suited to describe the event topology of two well-separated jets with little hadronic activity between them, as expected for events produced through vector boson fusion.

The remaining events are separated into four categories, defined by the $|\eta|$ of the photons in the calorimeter and the p_{Tt} of the event.

Figure 9 shows the different event categories, and their expected composition for the $\sqrt{s} = 8\,\text{TeV}$ analysis, as expected in the SM.

Figure 10 shows the signal strengths measured for the five production modes[3], where the signal strength is defined as the ratio of the measured number of events in a given production mode to the number of events expected from the SM. The measurements agree with the expectation from the SM within the present uncertainties. The inclusive signal strength is measured to be $\mu = 1.17 \pm 0.23\,(\text{stat})^{+0.10}_{-0.08}\,(\text{syst})^{+0.12}_{-0.08}\,(\text{theo})$. The largest contribution to the systematic uncertainty comes from the measurement of the photon energy resolution.

8. Measurement of differential cross sections

The measurement of differential cross sections allows to make an almost model-independent measurement of

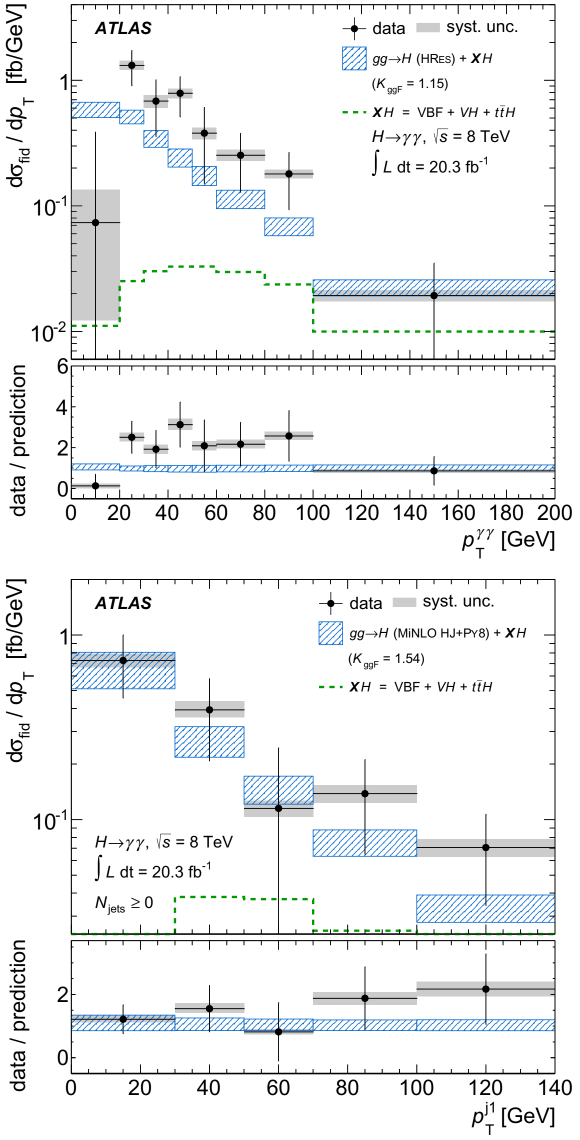

Figure 11: Transverse momentum of the diphoton pair (top) and of the leading jet (bottom) in $H \to \gamma\gamma$ events [6]. The data is shown as data points, with the systematic uncertainty indicated by the shaded area. The MC prediction (combining all production processes) with its uncertainty is shown by the hatched area. The contribution from the non-gluon fusion processes is shown as dashed line. The lower plots show the data-to-MC ratios.

---

[3] These proceedings present the results published in Ref. [5], which became available shortly after ICHEP 2014.

the Higgs boson production and decay kinematics, and the results can be compared to predictions. This allows, for example, a test of the simulation of the diphoton transverse momentum, which is an important ingredient in the mass and couplings measurements (see Secs. 6 and 7), or the production of jets together with a Higgs boson, which is an important ingredient in the coupling measurements in $H \to \gamma\gamma$ (see Sec. 7) and other decay channels.

The $H \to \gamma\gamma$ decay is well-suited for the measurement of differential cross sections due to its good mass resolution, allowing for a simple background subtraction, and the high signal yield. The measured cross sections are unfolded for detector acceptance, resolution and efficiency, and the unfolding is performed to a fiducial volume defined by $E_T > 0.35(0.25)m_{\gamma\gamma}$ for the leading (subleading) photon, $|\eta| < 2.37$ for the two photons, and jet rapidities smaller than 4.4.

Figure 11 shows the spectra of the diphoton transverse momentum, and the transverse momentum of the leading jet in $H \to \gamma\gamma$ events. A good agreement of the predictions with the measurements is observed within the uncertainties, which are dominated by the statistical uncertainties.

9. Conclusions

The past two years have seen a successful transition from Higgs boson searches to the measurements of the properties of the new particle. Precise measurements of its mass have been carried out, as well as first measurements of its couplings to SM particles and of differential cross sections. Most of these measurements are currently limited by the statistical precision of the data. This is also thanks to the significant effort that has been put into improving the energy calibration, as well as the measurement of the photon identification efficiency. A similar effort will be required for Run 2 in order to improve the precision of the property measurements with the expected larger data sets.

References

[1] The ATLAS Collaboration, Phys. Lett. B **716**, 1 (2012) [arXiv:1207.7214 [hep-ex]].

[2] S. Chatrchyan *et al.* [CMS Collaboration], Phys. Lett. B **716**, 30 (2012) [arXiv:1207.7235 [hep-ex]].

[3] The ATLAS Collaboration, JINST **3**, S08003 (2008).

[4] The ATLAS Collaboration, Phys. Rev. D **90**, 052004 (2014) [arXiv:1406.3827 [hep-ex]].

[5] The ATLAS Collaboration, arXiv:1408.7084 [hep-ex].

[6] The ATLAS Collaboration, JHEP09(2014)112 [arXiv:1407.4222 [hep-ex]].

[7] R. Fruehwirth, Comp. Phys. Comm. **154** (2003).

[8] The ATLAS Collaboration, https://atlas.web.cern.ch/Atlas/GROUPS/PHYSICS/EGAMMA/PublicPlots/20120620/PhotonRecoStability/ATL-COM-PHYS-2012-823/index.html.

[9] The ATLAS Collaboration, Phys. Rev. D **85**, 012003 (2012) [arXiv:1107.0581 [hep-ex]].

[10] The ATLAS Collaboration, ATLAS-CONF-2012-123.

[11] The ATLAS Collaboration, https://atlas.web.cern.ch/Atlas/GROUPS/PHYSICS/EGAMMA/PublicPlots/20140611/ATL-COM-PHYS-2014-542/index.html.

[12] The ATLAS Collaboration, ATLAS-CONF-2012-168.

[13] The ATLAS Collaboration, Phys. Lett. B **726**, 88 (2013) [arXiv:1307.1427 [hep-ex]].

[14] The ATLAS Collaboration, arXiv:1407.5063 [hep-ex].

[15] The ATLAS Collaboration, Eur. Phys. J. C **72**, 1909 (2012) [arXiv:1110.3174 [hep-ex]].

[16] OPAL Collaboration, [hep-ex/9710010].
M. Vesterinen and T.R. Wyatt, Nucl. Instrum. Meth. A602 (2009) [0807.4956 [hep-ex]].